

Construction Mechanism of a Basin of Attraction for Passive Dynamic Walking Induced by Intrinsic Hyperbolicity

Ippei Obayashi*

Department of Mathematics, Graduate School of Science
Kyoto University
Kitashirakawa Oiwakecho, Sakyo-ku, Kyoto 606-8502, Japan
Email: obayashi@math.kyoto-u.ac.jp

Shinya Aoi*

Department of Aeronautics and Astronautics, Graduate School of Engineering
Kyoto University
Kyoto daigaku-Katsura, Nishikyo-ku, Kyoto 615-8540
Japan
Email: shinya_aoi@kuaero.kyoto-u.ac.jp

Kazuo Tsuchiya*

Department of Aeronautics and Astronautics, Graduate School of Engineering
Kyoto University
Kyoto daigaku-Katsura, Nishikyo-ku, Kyoto 615-8540
Japan
Email: tsuchiya.k@nifty.com

Hiroshi Kokubu*

Department of Mathematics, Graduate School of Science,
Kyoto University
Kitashirakawa Oiwakecho, Sakyo-ku, Kyoto 606-8502
Japan
Email: kokubu@math.kyoto-u.ac.jp

Passive dynamic walking is a useful tool for investigating the mechanical functions of the body to produce energy-efficient walking. The basin of attraction is very small and thin, and it has a fractal-like shape; this explains the difficulty in producing stable passive dynamic walking. The underlying mechanism that produces these geometric characteristics was not known. In this paper, we use a simplest walking model to clarify the mechanism that forms the basin of attraction for passive dynamic walking from the viewpoint of dynamical systems theory. We show that the intrinsic saddle-type hyperbolicity of the upright equilibrium point in the governing dynamics plays an important role in the geometrical characteristics of the basin of attraction; this contributes to our understanding of the stability mechanism of bipedal walking.

1 Introduction

During human walking, the stance leg is almost straight, and it rotates around the foot contact point like an inverted pendulum. Therefore, the center of mass (COM) is at its highest position during the midstance phase and at its lowest position during the double-support phase. In contrast, the locomotion speed is lowest during the midstance phase and highest during the double-support phase. This means that humans produce efficient walking through the pendular exchange of potential and kinetic energy while conserving mechanical energy [1, 2, 3]. This is called the inverted pendulum mechanism [4], and inverted pendulums have been widely used as the simplest model for the movement of the COM, when investigating the underlying mechanism in human walking [5, 6, 7, 8, 9].

Passive dynamic walking, a popular dynamic system

that is based on the inverted pendulum mechanism, was proposed by McGeer [10, 11]. This system walks down a shallow slope without an actuator or controller by balancing the energy dissipation due to foot contact with the energy generation due to the gravitational potential energy. This walking behavior has various similarities to that of humans, and thus it has been a useful tool for elucidating the body's mechanical functions to produce energy-efficient walking [12, 13, 14, 15, 16, 17, 18, 19, 20, 21, 22, 23, 24, 25].

Due to the saddle property in the governing dynamics, the inverted pendulum easily falls down. Therefore, a crucial issue is to clarify the stability mechanism of passive dynamic walking. Garcia et al. [26] used a simple compass-type model that incorporated the swing leg into the inverted pendulum (the simplest walking model) and used a perturbation method to elucidate the generation of a stable limit cycle and the linear stability of the movement. The stability characteristics of dynamical systems are determined by the basin of attraction of attractors, as well as by the linear stability. Schwab and Wisse [27] investigated the basin of attraction of the simplest walking model and showed that it is very small and thin, and that it has a fractal-like shape; this explains the difficulty in producing stable passive dynamic walking. More detailed studies of the stability and bifurcation of the simplest walking model and similar compass-type models are made [28, 29, 30, 31]. However, it remains unclear what mechanisms induce these geometric characteristics in the basin of attraction.

In the present study, we aim to clarify the mechanism that determines the geometric characteristics of the basin of attraction of the simplest walking model by considering the theory of dynamical systems and focusing on the saddle point that is inherent in the governing dynamics. Because saddle property is embedded in general locomotor systems (they are not limited to passive dynamic walking), our results might contribute not only to elucidating the stability mechanism in passive dynamic walking, but also to improving the understanding of the stability mechanism in human walking and thus to producing design principles for the control of walking-support systems and biped robots.

2 Methods

2.1 Model

In this study, we use the simplest walking model (Fig. 1), introduced by Garcia et al. [26], for the dynamical analysis of passive dynamic walking. This model has two legs (rigid links), each of length l , connected by a frictionless hip joint. θ_1 is the angle of the stance leg with respect to the slope normal, and θ_2 is the angle between the stance leg and the swing leg. The mass is located only at the hip and the feet; the hip mass is M , and the foot mass is m . g is the acceleration due to gravity. This model walks on a slope of angle γ , without any control or input. To simplify the analysis, we consider the limit case $\beta = m/M \rightarrow 0$ as in [26].

In this paper, we show the model briefly. Please see [26] for the detailed explanation of the model.

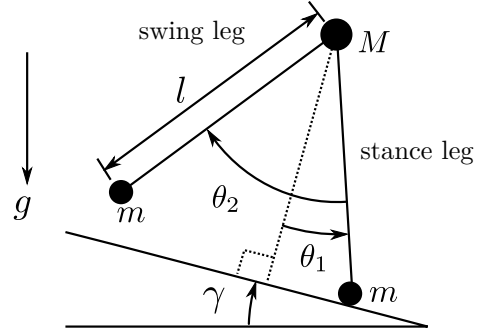


Fig. 1. Simplest walking model

2.1.1 Equations of motion for the swing phase

The configuration of the model is described by two variables (θ_1, θ_2) in Fig. 1. The equations of motion are as follows:

$$\ddot{\theta}_1 - \sin(\theta_1 - \gamma) = 0 \quad (1)$$

$$(\cos \theta_2 - 1)\ddot{\theta}_1 + \ddot{\theta}_2 - \dot{\theta}_1^2 \sin \theta_2 + \sin(\theta_2 - \theta_1 + \gamma) = 0. \quad (2)$$

In this equations, we have already take the limit $\beta = m/M \rightarrow 0$ and nondimensionalized the equations using the time scale $\sqrt{l/g}$.

2.1.2 Foot contact

The swing foot contacts the slope when the following conditions are satisfied:

$$2\theta_1 - \theta_2 = 0 \quad (3)$$

$$\theta_1 < 0 \quad (4)$$

$$2\dot{\theta}_1 - \dot{\theta}_2 < 0. \quad (5)$$

Conditions (4) and (5) are used to ignore the foot scuffing when the swing leg moves forward.

We assume that foot contact is a fully inelastic collision (no-slip, no-bound) and that the stance foot lifts off the slope as soon as the swing foot hits the slope. The relationship between the state just before foot contact $(\theta_1^-, \dot{\theta}_1^-, \theta_2^-, \dot{\theta}_2^-)$ and the state just after foot contact $(\theta_1^+, \dot{\theta}_1^+, \theta_2^+, \dot{\theta}_2^+)$ is as follows:

$$\begin{bmatrix} \theta_1^+ \\ \dot{\theta}_1^+ \\ \theta_2^+ \\ \dot{\theta}_2^+ \end{bmatrix} = \begin{bmatrix} -\theta_1^- \\ \dot{\theta}_1^- \cos 2\theta_1^- \\ -2\dot{\theta}_1^- \\ \cos 2\theta_1^- (1 - \cos 2\theta_1^-) \dot{\theta}_1^- \end{bmatrix}. \quad (6)$$

Since the state just after foot contact depends only on $(\theta_1^-, \dot{\theta}_1^-)$ and is independent of $(\theta_2^-, \dot{\theta}_2^-)$, it forms a two-dimensional surface in the four-dimensional phase space $(\theta_1, \dot{\theta}_1, \theta_2, \dot{\theta}_2)$.

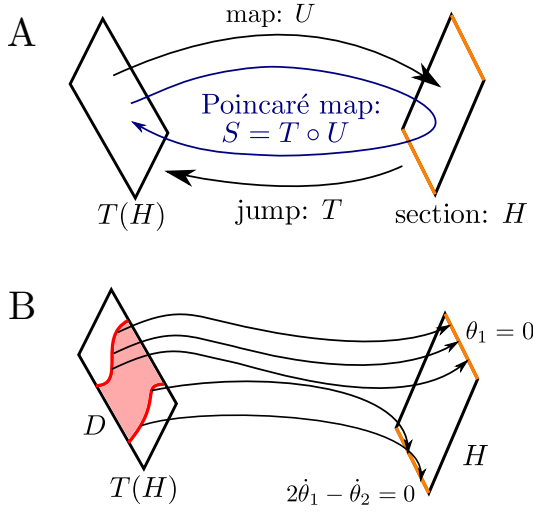


Fig. 2. Structure of phase space $(\theta_1, \dot{\theta}_1, \theta_2, \dot{\theta}_2)$. A: Foot contact condition (section) H bounded by two conditions (orange lines), the jump by foot contact T , the state just after foot contact event $T(H)$, the map from $T(H)$ to H by the equations of motion for the swing phase U , and the Poincaré map S defined by $S = T \circ U$ on the Poincaré section $T(H)$. B: Domain D (red region) bounded by the backward orbits of two boundaries of H by the equations of motion for the swing phase (red lines)

2.2 Structure of phase space by hybrid dynamics

The simplest walking model is a hybrid system composed of the continuous dynamics during the swing phase and the discontinuous dynamics at foot contact. The hybrid dynamics determines the structure of the phase space, as shown in Fig. 2A. H is the section of foot contact defined by the conditions (3), (4), and (5). T is the jump in the phase space from the state just before foot contact to the state just after foot contact, defined by the relationship (6). Therefore, the image of T , $T(H)$, is the region representing all states just after foot contact and a new step starts from $T(H)$. U is the map from the start of a step to the foot contact. In other words, U is the map from $T(H)$ to H , defined by the equations of motion (1) and (2). The Poincaré map S is defined by $S = T \circ U : T(H) \rightarrow T(H)$ on the Poincaré section $T(H)$. This Poincaré map represents one gait cycle, and an attractor of the Poincaré map represents stable walking. The basin of attraction of S is the main topic of this paper. S is parameterized by one parameter γ , and Garcia et al. [26] found that S has an attracting fixed point at $0 < \gamma < 0.015$, and there is a period-doubling cascade to chaos at $0.015 < \gamma < 0.019$.

To investigate the basin of attraction, the domain of T is important. The map S is not defined for all $T(H)$, since the model may fall down from some initial conditions. We define the domain, D , by the collection of initial conditions on which the model takes at least one step. D is in $T(H)$ and bounded, as shown in Fig. 2B. H has two boundaries (orange lines) defined by $\theta_1 = 0$ and $2\dot{\theta}_1 - \dot{\theta}_2 = 0$ from the conditions (4) and (5), and the backward flows of these boundaries by the equations of motion (1) and (2) determine the boundaries of D (red lines).

We also consider the sequence of inverse images of D ,

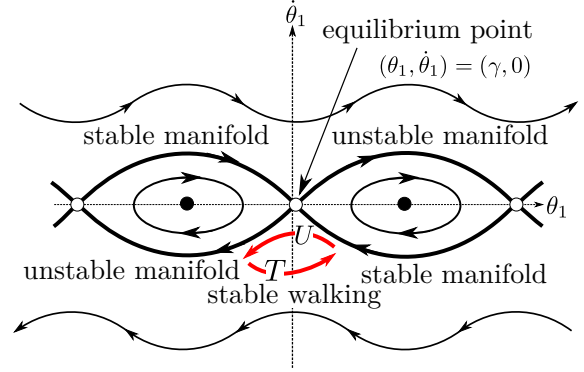


Fig. 3. Phase diagram $(\theta_1, \dot{\theta}_1)$. The equilibrium point $(\theta_1, \dot{\theta}_1) = (\gamma, 0)$ is a saddle. Stable walking is obtained by the map U and the jump T .

$S^{-n}(D)$ ($n = 1, 2, \dots$). These regions indicate the collections of initial conditions on which the model takes at least two steps, three steps, \dots . The sequence approximates the basin of attraction, and we investigate the mechanism by which the shape of the basin of attraction is formed from the geometric structure of these inverse images.

2.3 Hyperbolicity and manifolds of the governed equations

The equations of motion (1) and (2) have an equilibrium point $(\theta_1, \dot{\theta}_1, \theta_2, \dot{\theta}_2) = (\gamma, 0, 0, 0)$. At the equilibrium point, the legs remain upright. The equilibrium point is deeply related to the geometric structure of the basin of attraction, which we will discuss in the following sections. The eigenvalues of the linearized equations of motion at the equilibrium point are ± 1 and $\pm i$, and the equilibrium point is a saddle-center with one stable direction, one unstable direction, and two neutral directions.

The changes in the angle of the stance leg θ_1 are governed by the equation (1) and are not affected by the movement of the swing leg θ_2 (this is because we are considering the limit case, $\beta \rightarrow 0$). This equation for θ_1 has a saddle equilibrium point at $(\theta_1, \dot{\theta}_1) = (\gamma, 0)$, as shown in Fig. 3, similar to that of a single inverted pendulum. In the phase diagram of $(\theta_1, \dot{\theta}_1)$ in Fig. 3, bold lines going into $(\gamma, 0)$ are the stable manifold of the equilibrium point W^s , and the bold lines going out of the equilibrium point are the unstable manifold of the equilibrium point W^u . In the phase space of four variables, $(\theta_1, \dot{\theta}_1, \theta_2, \dot{\theta}_2)$, $W^s \times \mathbb{R}^2$ and $W^u \times \mathbb{R}^2$ are the center stable manifold and the center unstable manifold, respectively, and we denote them by W^{cs} and W^{cu} . An orbit on W^{cs} behaves as follows (Fig. 4):

- An orbit starting from a point on W^{cs} never goes outside of W^{cs} ;
- An orbit starting from a point on W^{cs} converges to $(\gamma, 0) \times \mathbb{R}^2$ as $(\text{time}) \rightarrow +\infty$.

An orbit on W^{cu} behaves in the same way as one on W^{cs} , as $(\text{time}) \rightarrow -\infty$.

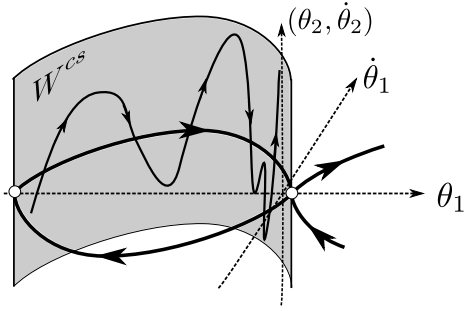


Fig. 4. Center stable manifold W^{cs}

2.4 Computation of regions and manifolds

To investigate the geometric structure of the basin of attraction, we compute the domain D , the sequence of inverse images of the domain $S^{-n}(D)$ ($n = 1, 2, \dots$), the basin of attraction B , and the intersection of W^{cs} and $T(H)$. All of these sets are defined on $T(H)$. The jump map (6) shows that $T(H)$ is a two-dimensional surface in the four-dimensional phase space \mathbb{R}^4 , and each point on $T(H)$ is uniquely determined by two variables $(\theta_1, \dot{\theta}_1)$. Therefore, we use the coordinates $(\theta_1, \dot{\theta}_1)$ to describe this region. Because D is a set of initial points on $T(H)$ that reach H through the equations of motion (1) and (2) (Fig. 2), we can compute D by numerically integrating the equations. We can also compute $S^{-n}(D)$ ($n = 1, 2, \dots$) in a similar way. We approximate B as a set of initial points on $T(H)$ that allows the model to take a sufficient number of steps. We compared the results using 50 and 200 steps and used them since the two results were identical. We can also compute the intersection of W^{cs} and $T(H)$ from the fact that W^{cs} is a separatrix of solutions, as shown in Figs. 3 and 4.

3 Results

Figure 5A shows the domain D and the basin of attraction B on $T(H)$ with $\gamma = 0.011$. Both D and B are very thin in the space of $(\theta_1, \dot{\theta}_1)$. To clearly see the geometrical details, we rotated the figure using $\theta_1 + \dot{\theta}_1$ and $\theta_1 - \dot{\theta}_1$ for the axis in Fig. 5B. The intersection of the center-stable manifold W^{cs} and $T(H)$ is shown by a green line in Figs. 5A and B. From these figures, we found that D had the following properties:

- D has a long, thin region in $(\theta_1, \dot{\theta}_1)$;
- Two boundaries of D are almost parallel, and one of them is very close to W^{cs} .

We also found the following properties for B :

- B is located inside D and is thinner than D ;
- B is V-shaped;
- There are fractal-like slits in B and a stripe pattern in the cusp of the V-shaped region.

To investigate how to generate these geometric characteristics of B from D , we calculated the inverse images of D , $S^{-n}(D)$ ($n = 1, 2, \dots$). Figure 6 shows D , $S^{-1}(D)$, and $S^{-2}(D)$. We found the following:

- $S^{-1}(D)$ is contained in D and is V-shaped;

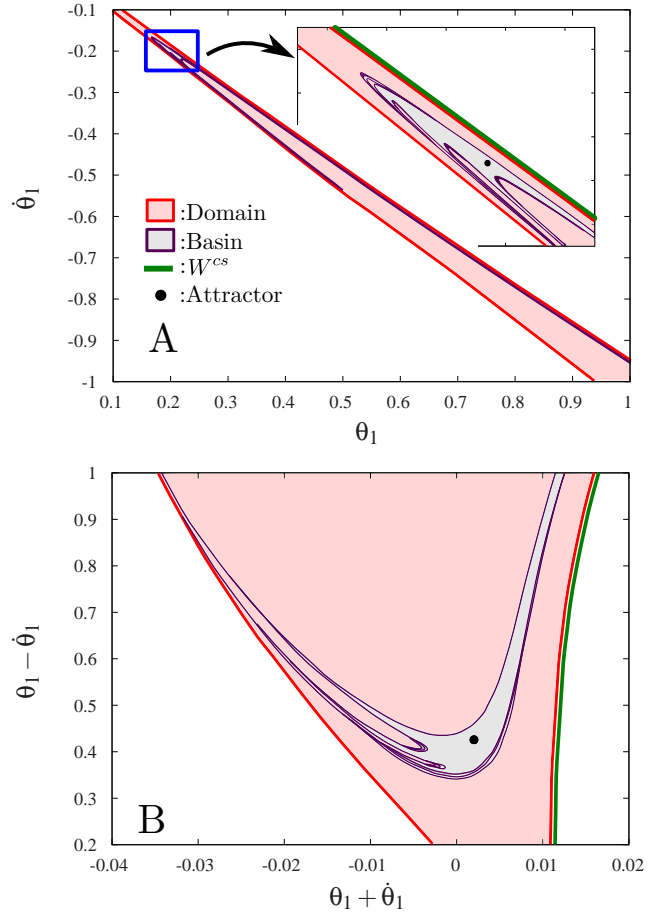


Fig. 5. Geometric characteristics of the basin of attraction for $\gamma = 0.011$. A: Domain D and basin of attraction B on $(\theta_1, \dot{\theta}_1)$. B: Magnified view (blue box in A). C: Rotated view using $\theta_1 + \dot{\theta}_1$ and $\theta_1 - \dot{\theta}_1$ for the axes.

- $S^{-2}(D)$ is located inside $S^{-1}(D)$, is V-shaped, and has a slit.

Figure 7 shows the inverse image $S^{-7}(D)$. A stripe pattern appears through the sequence of $S^{-n}(D)$ ($n = 1, 2, \dots$).

As shown in the above figures, B is constructed by the sequence of the backward images $S^{-n}(D)$ ($n = 1, 2, \dots$). Therefore, we can find the construction mechanism of the shape of the basin of attraction from the backward images; we will discuss this in Section 4.

To examine the dependence of the geometric characteristics on the parameter γ , we calculated the domain D , the basin of attraction B , and the inverse images $S^{-1}(D)$ and $S^{-2}(D)$ for various values of γ (Fig. 8). Figures 8A and B show the results for $\gamma = 0.016$ and have two attracting points, which correspond to a stable period-2 gait. Figures 8C and D show the results for $\gamma = 0.0178$ and have four attracting points, which correspond to a stable period-4 gait. Figures 8E and F show the results for $\gamma = 0.019$ and have a chaotic attractor. These figures show that B , D , $S^{-1}(D)$, and $S^{-2}(D)$ change somewhat depending on γ . When γ is larger than 0.019, the attractor disappears. We will discuss this “attractor crisis” phenomenon in Section 4.4.

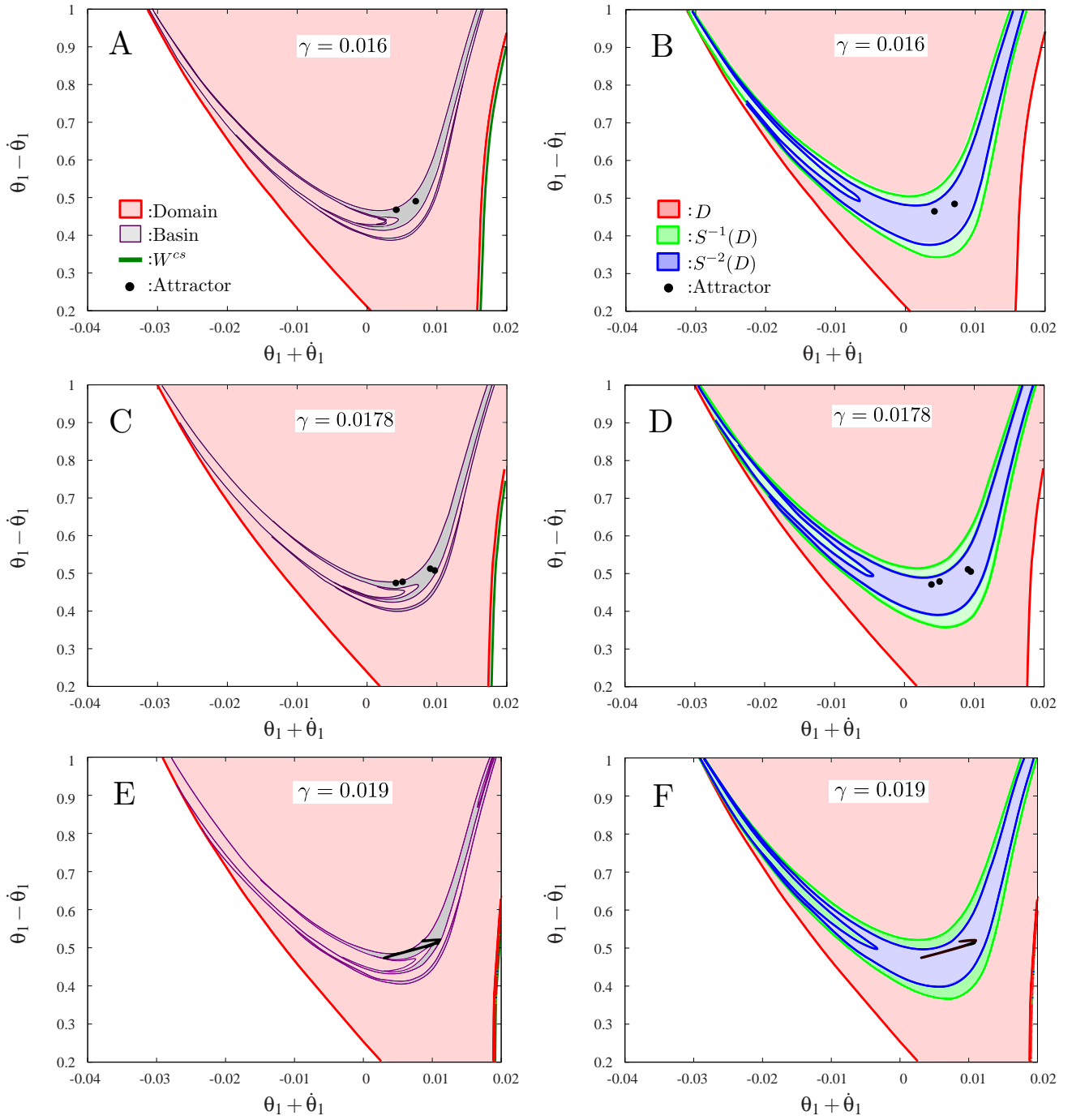


Fig. 8. Dependence of the parametric characteristics on the parameter γ . $\gamma = 0.016$ for A and B, 0.0178 for C and D, and 0.019 for E and F. A, C, and E show the domain D , the basin of attraction B , and the intersection with W^{cs} . B, D, and F show the domain D , and the inverse images $S^{-1}(D)$ and $S^{-2}(D)$.

4 Discussion

4.1 Why the domain is thin?

The domain D is very thin, as shown in Fig. 5A. This is related to the λ -lemma, one of the most important theorems in the theory of dynamical systems. From this theorem, we can say the following (see the textbook by Robinson [32] for the exact notation and a proof of the theorem):

- A region intersecting the unstable manifold of a saddle

equilibrium point moves toward the stable manifold of the saddle when the region is moved by the backward flow;

- When the region comes close to the stable manifold, the region becomes thin due to the hyperbolic behavior near the saddle.

Figure 12 illustrates how a region X moves and is deformed into thinner regions Y and Z . As shown in Fig. 2B, D is

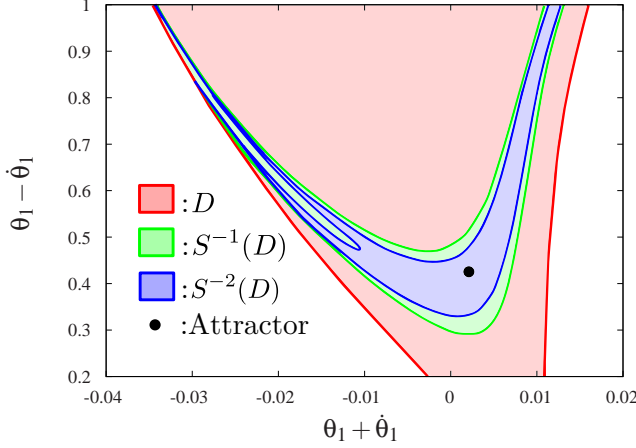


Fig. 6. Domain D and inverse images $S^{-1}(D)$ and $S^{-2}(D)$

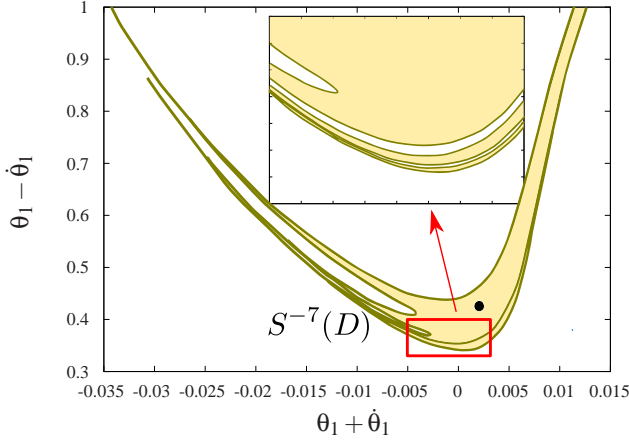


Fig. 7. A: Inverse image $S^{-7}(D)$, B: Magnified view (red box in A)

obtained by the intersection of $T(H)$ and the backward orbit whose initial point is in H . Therefore, D becomes thin along the center stable manifold, as shown in Figs. 5A and 12. This explains why the domain is very thin.

4.2 Why the inverse image of the domain is V-shaped?

Since the sequence of the inverse images $S^{-n}(D)$ ($n = 1, 2, \dots$) approximates the basin of attraction, it is important to clarify how the geometric structure of the inverse images is constructed, and hence the shape of the basin of attraction.

First, $S^{-1}(D)$ is V-shaped in the thin region D , as shown in Fig. 6. The construction of this shape is expressed as follows (Figs. 13A and B). D is a thin region along the center stable manifold, as described in Section 4.1. Since $S = T \circ U$, we have $S^{-1}(D) = U^{-1}(T^{-1}(D))$. From (6), $T^{-1}(D)$ is described as:

$$\{(-\theta_1^+, -2\theta_1^+, \dot{\theta}_1^+ \sec 2\theta_1^+, \dot{\theta}_2^-) \mid (\theta_1^+, \theta_2^+, \dot{\theta}_1^+, \dot{\theta}_2^+) \in D, \dot{\theta}_2^- \in \mathbb{R}\} \quad (7)$$

Numerically computed $T^{-1}(D)$ is shown in Fig. 9. The re-

gion is thin and curved, and away from the unstable manifold as θ_1 decreases. The relative position of $T^{-1}(D)$ and W^{cu} is important for V-shaped $S^{-1}(D)$ as expressed below.

To consider $S^{-1}(D) = U^{-1}(T^{-1}(D))$, we study the motion by U in detail. The map U is described as follows. We write $\Theta(t) = (\theta_1(t), \theta_2(t), \dot{\theta}_1(t), \dot{\theta}_2(t))$ as the solution of equations of motion. From the definition of U , for a point $\Theta(0) \in T^{-1}(D) \subset H$, there is $\Delta > 0$ such that

$$\Theta(-\Delta) = U^{-1}(\Theta(0)) \in T(H) \quad (8)$$

This $\Theta(0)$ is the state of foot contact, and $\Theta(-\Delta)$ is the state of just after foot contact, and Δ is the duration of a single support phase. Since $\Theta(-\Delta)$ is contained in $T(H)$, the following two equations hold:

$$\begin{aligned} 2\theta_1(-\Delta) &= \theta_2(-\Delta) \\ \dot{\theta}_2(-\Delta) &= \dot{\theta}_1(-\Delta)(1 - \cos 2\theta_1(-\Delta)). \end{aligned}$$

Since $\Theta(-\Delta)$ is contained in H , the following equation holds:

$$2\theta_1(0) = \theta_2(0).$$

We can compute U this system of equations. To analyze U , we introduce some approximations.

We consider the linearized equation of (1)(2) around $(\gamma, 0, 0, 0)$ as an approximation of $\Theta(t)$. The solution of the linearized equations is:

$$\begin{aligned} \theta_1 &= \gamma + C_1 \exp(t) + C_2 \exp(-t) \\ \theta_2 &= K \cos(t + \phi) + \theta_1/2. \end{aligned} \quad (9)$$

where C_1, C_2, K, ϕ are the integration constant ($0 \leq \phi < 2\pi$). In addition, we introduce the approximation of $\theta_1(-\Delta) \approx -\dot{\theta}_1(-\Delta)$ since $\Theta(-\Delta) \in D$ and D is a thin region along with W^{cs} . Using these approximations, we derive the system of equations:

$$\begin{aligned} \theta_1(-\Delta) &= C_1 \exp(-\Delta) + C_2 \exp \Delta + \gamma \\ K \cos(-\Delta + \phi) &= 3\theta_1(-\Delta)/2 \\ K \sin(-\Delta + \phi) &= -\theta_1(-\Delta)(1/2 - \cos 2\theta_1(-\Delta)) \\ K \cos \phi &= 2(C_1 + C_2 + \gamma) \end{aligned} \quad (10)$$

where $\Delta, \phi, K, \theta_1(-\Delta)$ are the unknown variables and C_1, C_2 are the parameters. We can compute $\Theta(-\Delta) = U^{-1}(\Theta(0))$ from $(\theta_1(0), \dot{\theta}_1(0))$ since $C_1 = (\theta_1(0) - \gamma + \dot{\theta}_1(0))/2$, $C_2 = (\theta_1(0) - \gamma - \dot{\theta}_1(0))/2$. C_2 is the approximated distance between $\Theta(0)$ and W^{cu} , and C_2 is important for the deformation of $T^{-1}(D)$ by U^{-1} .

To study how to deform $T^{-1}(D)$ by U^{-1} , take a line seg-

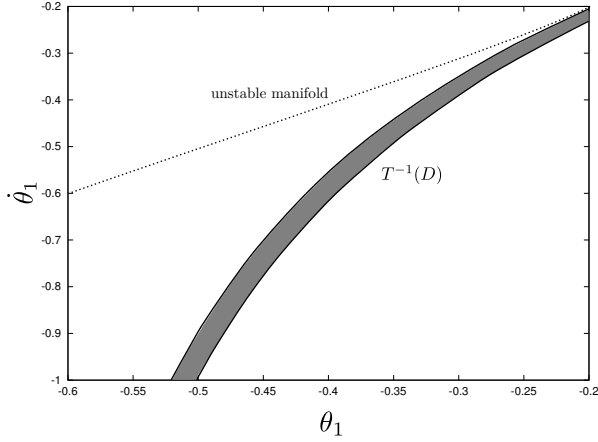


Fig. 9. $T^{-1}(D)$ and W^{cu}

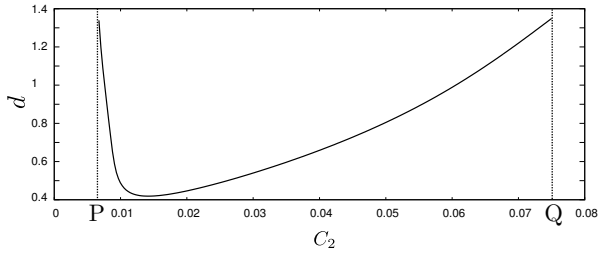


Fig. 10. Distance C_2 between the point on the line PQ and E^u versus distance d between the point projected from the line PQ by U^{-1} and E^u

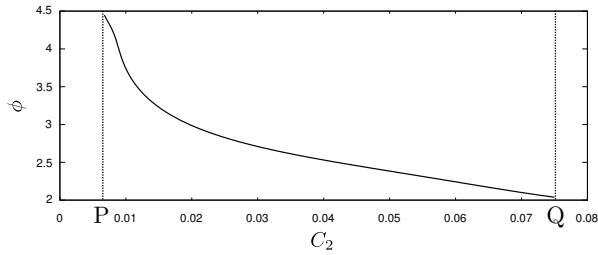


Fig. 11. C_2 versus ϕ

ment PQ in Fig. 9 and study the curve $P'Q' = U^{-1}(PQ)$. The segment PQ is parameterized by C_2 , the distance between a point on PQ and the unstable vector (the line $E^u : \theta_1 = \bar{\theta}_1 - \gamma$). Figure 10 shows the C_2 versus d , where d is the distance between $\Theta(-\Delta)$ and E^u . The curve is convex, and this fact means that $T^{-1}(D)$ is nonuniformly deformed by U^{-1} as in Fig. 13B. The part of $T^{-1}(D)$ very close to W^{cu} (around P) and the part of $T^{-1}(D)$ far from W^{cu} (around Q) are strongly expanded by U^{-1} , and the intermediate part is relatively weakly expanded. Therefore, $U^{-1}(T^{-1}(D)) = S^{-1}(D)$ is V-shaped. We need to explain why the curve in Fig. 10 is convex.

First, we consider the case of very small C_1 . From the equations (10), we have the following equation.

$$\tan(-\Delta + \phi) = -2(1/2 - \cos 2\theta_1(-\Delta))/3 \quad (11)$$

From $-1 \leq \cos 2\theta_1(-\Delta) \leq 1$, we have

$$-1 \leq \tan(-\Delta + \phi) \leq 1 \quad (12)$$

and we have $|\cos(-\Delta + \phi)| \geq 1/\sqrt{2}$. Therefore,

$$\begin{aligned} C_2 \exp \Delta &\geq \theta_1(-\Delta) - \gamma \\ &= (2/3) \cdot |K| |\cos(-\Delta + \phi)| - \gamma \\ &\geq (2/3) \cdot 2|(C_1 + C_2 + \gamma)/\cos \phi| \cdot (1/\sqrt{2}) - \gamma \\ &\geq (2\sqrt{2}/3) \cdot |C_1 + C_2 + \gamma| - \gamma. \end{aligned}$$

Since γ is small (0.011), Δ goes to $+\infty$ as $C_2 \rightarrow 0$. Δ tends to increase as C_2 become small.

From (12), Δ must satisfy the condition $-\pi/4 < -\Delta + \phi + \pi k < \pi/4$ ($k = 0, \pm 1, \dots$). In this paper, we only consider the case of $k = 0$ (we can discuss other cases in a similar way). Since $\Delta - \pi/4 < \phi < \Delta + \pi/4$ and $\Delta \rightarrow \infty$ as $C_2 \rightarrow 0$, ϕ goes to ∞ . However, $\phi \neq \pi/2, 3\pi/2$ from the first equation of (10). This means that the solution of (10) has a singularity and ϕ goes to $\pi/2$ or $3\pi/2$ as the solution goes to the singularity. We can numerically compute the singularity on the segment PQ in Fig. 11. ϕ goes to $3\pi/2$ as C_2 decreases. As a result, $|K|$ goes to $+\infty$ as $\phi \rightarrow 3\pi/2$ since $K = 2|C_1 + C_2 + \gamma|/\cos \phi$ holds. This causes that $\theta_1(-\Delta) = 2|K \cos(-\Delta + \phi)|/3$ become large. Since $d \approx \sqrt{2} \cdot \theta_1(-\Delta)$, d also become large.

Intuitively, we explain the phenomenon as follows. When C_2 is very small, $(\theta_1(t), \dot{\theta}(t))$ passes through the small neighborhood of the saddle equilibrium point. Therefore, the motion becomes slow and Δ becomes large. To adjust the time of foot contact, the motion of the swing leg become larger, and d become larger.

Next, we consider the case of large C_2 . In this case, Δ is not so large since the orbit does not pass through the neighborhood of the saddle equilibrium point. Therefore, C_2 is dominant for $\theta_1(-\Delta)$ and $d \approx \sqrt{2} \cdot \theta_1(-\Delta)$ since $\theta_1(-\Delta) = C_1 \exp(-\Delta) + C_2 \exp \Delta + \gamma$. So d becomes larger when C_2 becomes larger.

Integrating the above two cases, The part of $T^{-1}(D)$ very close to W^{cu} (around P) and the part of $T^{-1}(D)$ far from W^{cu} (around Q) are strongly deformed and the intermediate part is weakly deformed. This is because $S^{-1}(D)$ is V-shaped.

4.3 Why the inverse images have slits and stripe patterns?

We can also explain why the inverse image $S^{-2}(D)$ has a slit in the same way (Figs. 13C and D). Since $S^{-2}(D) = U^{-1}(T^{-1}(S^{-1}(D)))$, we consider two steps, $T^{-1}(S^{-1}(D))$ and $U^{-1}(T^{-1}(S^{-1}(D)))$. $T^{-1}(S^{-1}(D))$ is obtained by the backward image of $S^{-1}(D)$, and it is contained in $T^{-1}(D)$, shown as the blue region in Fig. 13C. The region is moved by U^{-1} and expanded along the direction of the stable manifold and contracted along the direction of the unstable manifold, as with $T^{-1}(D)$. Finally, $S^{-2}(D)$ becomes V-shaped with a

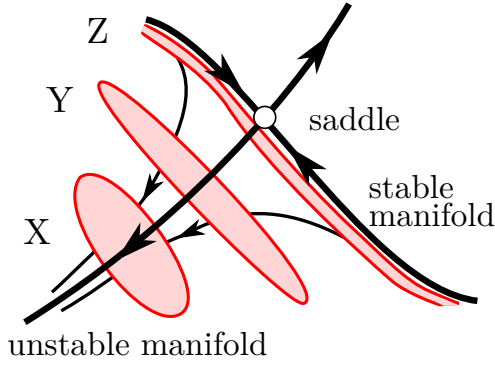


Fig. 12. λ -lemma. Region X moves and is deformed to thinner regions Y and Z by the backward flow. In our model, the foot contact section H and domain D correspond to the regions X and Z, respectively.

slit, as shown in Fig. 13D. We can also give a similar explanation for the stripe pattern, which is formed by the repeated expansion of nested regions.

4.4 Why the attractor disappears?

In the above discussion, we clarified the mechanism that shapes the basin of attraction. Although the parameter γ induces a period-doubling cascade to chaos, the mechanism for constructing the basin of attraction is the same and does not depend on γ . The domain, the inverse images of the domain, and the basin of attraction have only continuous changes that depend on γ , as shown in Fig. 8. Figures 14A and B show the basin of attraction and the chaotic attractor for $\gamma = 0.0187$ and 0.01903, respectively, before the attractor disappears. The attractor expands to reach the boundaries of the basin of attraction, as γ increases. When the attractor contacts the boundaries of the basin of attraction (red arrows in Fig. 14B), the attractor breaks down and the model ceases to walk. This phenomenon is known as the boundary (attractor) crisis [33].

5 Conclusion

In the present study, we clarified the construction mechanism for the basin of attraction for passive dynamic walking by focusing on the intrinsic hyperbolicity in the governing dynamics and using the viewpoint of the theory of dynamical systems. We used the foot contact section H , the jump map T , the domain D (the region on $T(H)$ where the model takes at least one step), the center stable and center unstable manifolds, the Poincaré map S , and the inverse maps. Our results showed that the basin of attraction is determined by the relative positions of the center unstable manifold and $T^{-1}(D)$, and the hyperbolicity near the saddle. The equilibrium point and the manifolds are determined only by the continuous equations of motion, and they are independent of the foot-contact condition. On the other hand, the positions of the domain and section are determined by the foot-contact condition and the jump map. These inherent hybrid dynamics clarified the mechanism for constructing the basin of attraction, and concepts from the theory of dynamical systems,

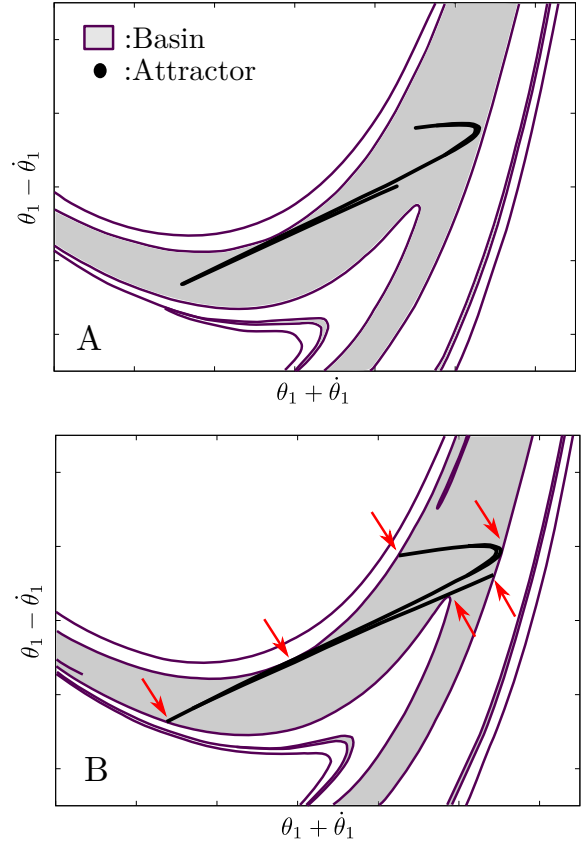


Fig. 14. Geometric relationship between the chaotic attractor and the basin of attraction for $\gamma = 0.0187$ (A) and 0.01903 (B)

such as the center stable/unstable manifolds, are very useful for the analysis of dynamic walking.

The thin, fractal-like basin of attraction of the simplest walking model is closely related to the one-dimensional instability of the upright equilibrium. Because an inverted pendulum is governed by such a saddle-type instability, it plays important roles in the generation of various whole-body movements, such as body sway in quiet standing [34, 35], as well as bipedal walking. Although the present study focused on passive dynamic walking, our result is not specific to it, but is widely applicable to general bipedal walking due to the intrinsic saddle property.

However, we note that the V-shaped basin of attraction, the slits, and the stripe patterns are formed by the relative positions of the center unstable manifold and $T^{-1}(D)$, and the hyperbolicity near the saddle, as shown in Fig. 13. Therefore, different bipedal walking models may have different shapes for the basin of attraction, depending on the relative positions. However, these elements have similar properties among bipedal walking models due to the intrinsic saddle-type hyperbolicity, so the discussion for these models may proceed in a similar way to those for our model. Therefore, the present study may contribute not only to elucidating the stability mechanism in passive dynamic walking, but also to improving the understanding of the stability mechanism in human walking and to producing design principles for the control of walking support systems and biped robots.

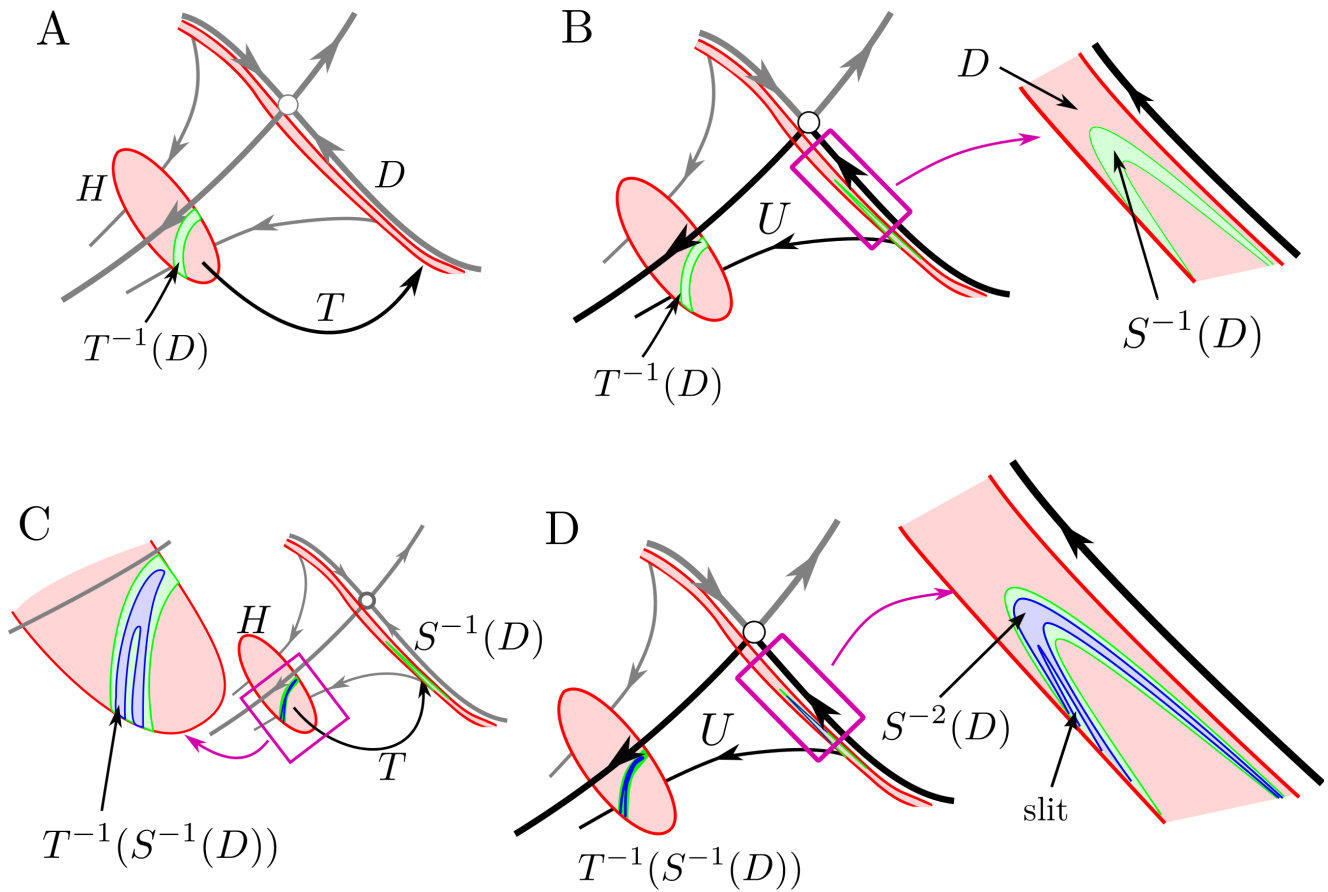


Fig. 13. Mechanism on how the inverse images of the domain are V-shaped and have slits. A: $T^{-1}(D)$ is obtained by the inverse image of D and becomes a thin and curved region in H . B: $T^{-1}(D)$ is moved and deformed by the backward flow to $S^{-1}(D) = U^{-1}(T^{-1}(D))$. C: $T^{-1}(S^{-1}(D))$ is obtained by the inverse image of $S^{-1}(D)$. D: $T^{-1}(S^{-1}(D))$ is moved and deformed by the backward flow to $S^{-2}(D) = U^{-1}(T^{-1}(S^{-1}(D)))$.

In our future study, based on the geometrical characteristics clarified in this paper, we intend to improve the stability of bipedal walking by manipulating the relative positions of the center unstable manifold and $T^{-1}(D)$ by designing a control system for a passive dynamic walking model.

References

- [1] Cavagna, G. A., Saibene, F. P., and Margaria, R., 1963. "External work in walking". *Journal of Applied Physiology*, **18**(1), pp. 1–9.
- [2] Cavagna, G. A., and Margaria, R., 1966. "Mechanics of walking". *Journal of Applied Physiology*, **21**(1), pp. 271–278.
- [3] Cavagna, G. A., Heglund, N. C., and Taylor, C. R., 1977. "Mechanical work in terrestrial locomotion: two basic mechanisms for minimizing energy expenditure". *American Journal of Physiology - Regulatory, Integrative and Comparative Physiology*, **233**(5), pp. R243–R261.
- [4] Ogiwara, N., Aoi, S., Sugimoto, Y., Tsuchiya, K., and Nakatsukasa, M., 2011. "Forward dynamic simulation of bipedal walking in the Japanese macaque: Investigation of causal relationships among limb kinematics, speed, and energetics of bipedal locomotion in a non-human primate". *American Journal of Physical Anthropology*, **145**(4), pp. 568–580.
- [5] Alexander, R., 1980. "Mechanics of bipedal locomotion". In *Perspectives in Experimental Biology I*, P. Spencer-Davies, ed. Oxford: Pergamon Press, pp. 493–504.
- [6] Mochon, S., and McMahon, T. A., 1980. "Ballistic walking". *Journal of Biomechanics*, **13**(1), pp. 49–57.
- [7] Mochon, S., and McMahon, T. A., 1980. "Ballistic walking: an improved model". *Mathematical Biosciences*, **52**(3-4), pp. 241–260.
- [8] Kuo, A. D., 2001. "A simple model of bipedal walking predicts the preferred speed-step length relationship". *ASME Journal of Biomechanical Engineering*, **123**(3), pp. 264–269.
- [9] Kuo, A. D., 2001. "Energetics of actively powered locomotion using the simplest walking model". *ASME Journal of Biomechanical Engineering*, **124**(1), pp. 113–120.
- [10] McGeer, T., 1990. "Passive dynamic walking". *The International Journal of Robotics Research*, **9**(2), pp. 62–82.
- [11] McGeer, T., 1993. "Dynamics and control of bipedal

- locomotion". *Journal of Theoretical Biology*, **163**(3), pp. 277–314.
- [12] Asano, F., Luo, Z.-W., and Yamakita, M., 2005. "Biped gait generation and control based on a unified property of passive dynamic walking". *IEEE Transactions on Robotics*, **21**(4), pp. 754–762.
- [13] Bruijn, S. M., Bregman, D. J. J., Meijer, O. G., Beek, P. J., and van Dieën, J. H., 2011. "The validity of stability measures: A modelling approach". *Journal of Biomechanics*, **44**(13), pp. 2401–2408.
- [14] Chyou, T., Liddell, G. F., and Paulin, M. G., 2011. "An upper-body can improve the stability and efficiency of passive dynamic walking". *Journal of Theoretical Biology*, **285**(1), pp. 126–135.
- [15] Russell, S., Sheth, P., and Granata, K. P., 2005. "Virtual slope control of a forward dynamic bipedal walker". *ASME Journal of Biomechanical Engineering*, **127**(1), pp. 114–122.
- [16] Coleman, M. J., and Ruina, A., 1998. "An uncontrolled walking toy that cannot stand still". *Physical Review Letters*, **80**(16), pp. 3658–3661.
- [17] Collins, S., Ruina, A., Tedrake, R., and Wisse, M., 2005. "Efficient bipedal robots based on passive-dynamic walkers". *Science*, **307**(5712), pp. 1082–1085.
- [18] Collins, S. H., Wisse, M., and Ruina, A., 2001. "A three-dimensional passive-dynamic walking robot with two legs and knees". *The International Journal of Robotics Research*, **20**(7), pp. 607–615.
- [19] Goswami, A., Thuilot, B., and Espiau, B., 1998. "A study of the passive gait of a compass-like biped robot: Symmetry and chaos". *The International Journal of Robotics Research*, **17**(12), pp. 1282–1301.
- [20] Johnston, T. R., and Hubbard, M., 2012. "Optimization of the visco-elastic parameters describing the heel-region of a prosthesis". *Journal of Theoretical Biology*, **311**, pp. 1–7.
- [21] Kuo, A. D., 1999. "Stabilization of lateral motion in passive dynamic walking". *The International Journal of Robotics Research*, **18**(9), pp. 917–930.
- [22] Kurz, M. J., Judkins, T. N., Arellano, C., and Scott-Pandorf, M., 2008. "A passive dynamic walking robot that has a deterministic nonlinear gait". *Journal of Biomechanics*, **41**(6), pp. 1310–1316.
- [23] Kwan, M., and Hubbard, M., 2007. "Optimal foot shape for a passive dynamic biped". *Journal of Theoretical Biology*, **248**(2), pp. 331–339.
- [24] Roos, P. E., and Dingwell, J. B., 2010. "Influence of simulated neuromuscular noise on movement variability and fall risk in a 3D dynamic walking model". *Journal of Biomechanics*, **43**(15), pp. 2929–2935.
- [25] Su, J. L.-S., and Dingwell, J. B., 2007. "Dynamic stability of passive dynamic walking on an irregular surface". *ASME Journal of Biomechanical Engineering*, **129**(6), pp. 802–810.
- [26] Garcia, M., Chatterjee, A., Ruina, A., and Coleman, M., 1998. "The simplest walking model: Stability, complexity, and scaling". *ASME Journal of Biomechanical Engineering*, **120**(2), pp. 281–288.
- [27] Schwab, A. L., and Wisse, M., 2001. "Basin of attraction of the simplest walking model". In *ASME Design Engineering Technical Conferences*.
- [28] de Boer, T., Wisse, M., and van der Helm, F. C. T., 2010. "Virtual slope control of a forward dynamic bipedal walker". *ASME Journal of Biomechanical Engineering*, **132**(7), p. 071012.
- [29] Gritli, H., Khraief, N., and Belghith, S., 2012. "Period-three route to chaos induced by a cyclic-fold bifurcation in passive dynamic walking of a compass-gait biped robot". *Communications in Nonlinear Science and Numerical Simulation*, **17**(11), pp. 4356–4372.
- [30] Gritli, H., Belghith, S., and Khraief, N., 2012. "Intermittency and interior crisis as route to chaos in dynamic walking of two biped robots". *International Journal of Bifurcation and Chaos*, **22**(03), p. 1250056.
- [31] Li, Q., and Yang, X.-S., 2012. "New walking dynamics in the simplest passive bipedal walking model". *Applied Mathematical Modelling*, **36**(11), pp. 5262–5271.
- [32] Robinson, C., 2008. *Dynamical systems: Stability, symbolic dynamics, and chaos*. Studies in Advanced Mathematics. CRC Press, Boca Raton, FL.
- [33] Grebogi, C., Ott, E., and Yorke, J. A., 1983. "Crises, sudden changes in chaotic attractors, and transient chaos". *Physica D*, **7**(1-3), pp. 181–200.
- [34] Suzuki, Y., Nomura, T., Casadio, M., and Morasso, P., 2012. "Intermittent control with ankle, hip, and mixed strategies during quiet standing: A theoretical proposal based on a double inverted pendulum model". *Journal of Theoretical Biology*, **310**, pp. 55 – 79.
- [35] Asai, Y., Tasaka, Y., Nomura, K., Nomura, T., Casadio, M., and Morasso, P., 2009. "A model of postural control in quiet standing: Robust compensation of delay-induced instability using intermittent activation of feedback control". *PLoS ONE*, **4**(7), 07, p. e6169.